International Journal of Multiphase Flow 36 (2010) 119–126

Contents lists available at ScienceDirect

International Journal of Multiphase Flow

journal homepage: www.elsevier.com/locate/ijmulflow

Review

Research on multiphase flows in Thermo-Energy Engineering Institute of Southeast University

Zhengbiao Peng, Zhulin Yuan *, Tie Li, Jie Cai, Xuan Wu, Fengxian Fan

Thermo-Energy Engineering Institute, School of Energy & Environment, Southeast University, Nanjing 210096, China

ARTICLE INFO

Article history:
Received 13 October 2008
Received in revised form 28 March 2009
Accepted 29 March 2009
Available online 12 April 2009

Keywords:
Multiphase flows
Mathematical modeling
Experimental study

ABSTRACT

Multiphase flows have received increasing attention over the past decades. This paper describes the research carried out in Thermo-Energy Engineering Institute of Southeast University in recent years, focusing on several common issues associated with multiphase flows in industry, such as: boiling of falling film and complex structure of gas–liquid flow under large difference in temperature, free surface flows involving liquid jets and drop formation, mixing behaviors of gas–liquid–solid three-phase flow, and fluidization characteristics of cylindrical particles. Numerical methods ranging from empirical to CFD models were developed for predictions, and experimental works were essentially conducted for validation and modification. For all cases, simulated results were validated with experiments and good agreements were obtained. Based on the combined modeling and experimental approach, fundamental understanding of multiphase processes in a specific circumstance is achieved under conditions relevant to the actual industrial-scale, such as transport phenomena, flow patterns, fluid dynamics and interactions between phases.

1. Introduction

Multiphase flows, i.e. flows involving more than one of the phases of matter-gas, liquid or solid, can be found in many industrial processes (Brennen, 2005). Research carried out in Thermo-Energy Engineering Institute (TEEI) of Southeast University in recent years has largely focused on the relevant topics in the field of multiphase flow, from fundamental study to applied investigations. As a general approach in the research on multiphase flows, numerical study on the detailed behavior of those flows and the phenomena that they manifest was adopted extensively in TEEI, to circumvent the difficulties inherent in the implementation of experimental investigations and reduce the cost in operation. Essentially, experiments were carried out for validation and modification. Up to now, robust mathematical models have already been established for the solution of force interaction between the dispersed (solid, liquid or gaseous) particles, both visible and invisible, using approaches ranging from discrete element model (DEM) (Tsuji et al., 1993; Yuan, 2000; Dhanunjay, 2003) to direct simulation Monte-Carlo (DSMC) method (Tsuji et al., 1998; Le and Hassan, 2007; Zou et al., 2008). Based on the Euler–Lagrange and Euler–Euler approaches, a series of research related to multiphase flow was carried out, including granular flows: particle-laden fluid–solid flow, cylindrical particles fluidization and ultra-fine particles removal, and multi-fluid flows: free surface flows and mixing behavior of multi-fluid flows. Moreover, studies of some advanced mathematical models are engaged for the solution of multiphase flows, such as lattice-Boltzmann model (LBM), large eddy simulation (LES) and multi-rigid dynamics model for simulation of non-spherical particles flows.

The objective of this paper is to give a brief summary of the research on multiphase flows carried out in TEEI in recent years, mainly including: boiling of the falling film and complex structure of gas–liquid flow under larger difference in temperature, free surface flows involving liquid jets and drop formation, mixing behavior of gas–liquid–solid three-phase flow, and fluidization behavior of cylindrical particles. Preliminary results extracted from the research are reviewed.

2. Boiling of falling film and complex structure of gas–liquid flow under larger difference in temperature

The falling film technique has been widely used in industrial sectors, among which the most important case is its application in the quenching chamber of Texaco gasifier. In the quenching chamber, water issuing out from the upper cooling ring falls along the inside wall and forms a thin film, which flows co-currently with the synthesis gas and molten slag produced in coal gasifier. Mass and heat are then transferred continuously and severely among the gas–liquid–solid phases under the large difference in temperature, as shown in Fig. 1. When the syngas with tempera-

* Corresponding author. Tel.: +86 25 85886060; fax: +86 25 57714489.
E-mail address: zlyuan@seu.edu.cn (Z. Yuan).

0301-9322/$ - see front matter © 2010 Published by Elsevier Ltd.
doi:10.1016/j.ijmultiphaseflow.2009.03.013

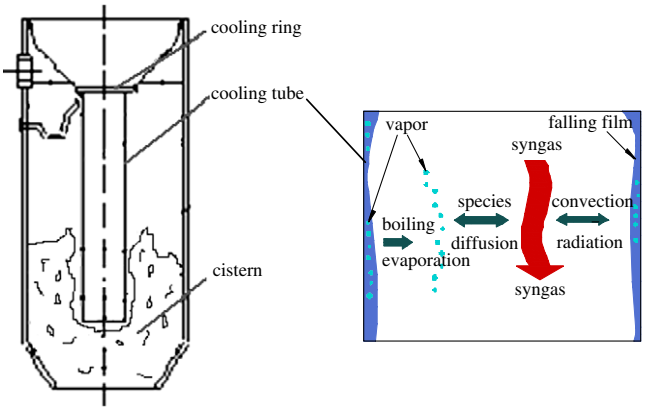

Fig. 1. Heat and mass transfer process in the downcomer.

ture generally higher than 1000 K is transported, the falling film inside the pipe is of great importance in avoiding wall burnout. However, the peculiar physical parameters thereof, such as fairly high temperature and high pressure always render the experimental explorations very difficult. Fortunately, with the great progresses in the computer technology, growing attention has been paid to numerical simulation study (Hiroki et al., 2008). Nevertheless, few relevant publications and reports are available currently to be referenced (Hughes and Bott, 1998; Tryggvason et al., 2005). In this section, a more fundamental study is carried out to understand the mechanisms governing the boiling process of falling film and the complex structure of gas–liquid flow, using a combined modeling and experimental approach.

2.1. Mathematical formulation

A two-dimensional model was developed to describe the multiphase flow. The mathematical model developed was the powerful technique of volume of fluid (VOF) (Liovic et al., 2002) integrated by the species transferred model (Marco, 1995). The governing equations satisfy the conservation laws of mass, momentum, energy and species. The continuity equation is given as:

$$\frac{\partial \alpha_q}{\partial t} + \nabla \cdot (\alpha_q \boldsymbol{v}_q) = \frac{S_q}{\rho_q}, \quad q = 1, 2 \tag{1}$$

where α is volume fraction of phase, $\boldsymbol{v}$ is the velocity vector, S is the mass source term. Subscript q denotes the qth phase.

Properties such as density and viscosity appearing in transport equations are determined by the volume fraction of each phase in a control volume. The VOF model solves throughout the domain the single momentum equation as:

$$\frac{\partial}{\partial t}(\rho \boldsymbol{v}) + \nabla \cdot (\rho \boldsymbol{v}\boldsymbol{v}) = -\nabla p + \rho \boldsymbol{g} + \nabla \cdot [\mu(\nabla \boldsymbol{v} + \nabla \boldsymbol{v}^T)] + \boldsymbol{F} \tag{2}$$

where ρ is the mixture density, and $\boldsymbol{F}$ is the momentum source term. The resulting velocity field is shared among the phases.

Cases are solved with species transported in the gas phase only. The species conservation equation is:

$$\frac{\partial}{\partial t}(\rho_V Y) + \nabla \cdot (\rho_V \boldsymbol{v} Y) = -\nabla \boldsymbol{J} + S_e \tag{3}$$

where Y and ρ_V represent the mass fraction and density of the water vapor, respectively. S_e is the mass source originating from the evaporation. $\boldsymbol{J}$ is diffusion flux of water vapor and can be modeled as:

$$\boldsymbol{J} = -\left(\rho_V D + \frac{\mu_t}{Sc_t}\right)\nabla Y \tag{4}$$

where D is vapor diffusion coefficient, Sc_t is turbulent Smith number, and μ_t is turbulent viscosity.

The energy equation is:

$$\frac{\partial}{\partial t}(\rho E) + \nabla \cdot [\boldsymbol{v}(\rho E + p)] = \nabla \cdot (k_{eff} \nabla T) + Q \tag{5}$$

Q is the energy source term accounting for the heat transfer via radiation, which is calculated by the Rossland model (Siegel and Howell, 1992); E and T denote the mass-averaged energy and temperature, respectively; k_{eff} is the effective thermal conductivity.

2.2. Experimental approach

A new type of coal–water–slurry (CWS) entrained-flow gasifier on a laboratory scale, consisting of the gasification section and the scrubbing–cooling chamber, was set up to validate the numerical results. In the measurement stage, the output signals of the thermocouples were converted into digital signals by ADAM data acquisition modules and transferred to a computer for analysis. Additionally, the monitor and control generated system (MCGS) configuration module was utilized in parallel to measure the temperature in real-time.

2.3. Results and discussion

Good agreement between the numerical and experimental results with respects to the axial temperature distribution in the pipe is shown in Fig. 2. To the point about 0.3 m below the inlet, the temperature has decreased to around 300 K. Good-quantity material of the upper region of the pipe is thus essential to resist the high temperature. From Fig. 2, it can be seen that there is a remarkable difference in shape of the two curves (experiment versus simulation) for locations below 20 cm from inlet. Analyses were done as follows. The water vapor resulting from phase change yields an increase in radiative capacity of the gas medium and hence enhances the radiative heat transfer in the vertical pipe. Consequently, gas temperature decreases more in experiments. However, this time-dependent behavior of radiative capacity was not considered for the simplified model. Accordingly, the temperature in simulations is higher than in experiments.

Fig. 3 shows the gas–liquid structure as a term of the volume fraction distribution of the syngas in the vertical pipe under the conditions both with and without phase change. In the case of "without phase change", the surface of the falling film is fairly smooth and continuous, whereas in the case of phase change occurring, the stability and continuity of the film are destroyed severely. Moreover, from Fig. 3(b–e), it can be found that higher gas inlet temperature is accompanied by more obvious film instability and discontinuity. The length of the continuous film decreases as

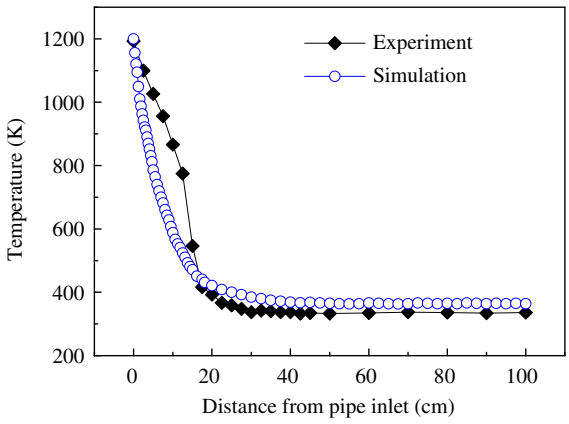

Fig. 2. Comparison of predicted and experimental results on axial temperature distribution.

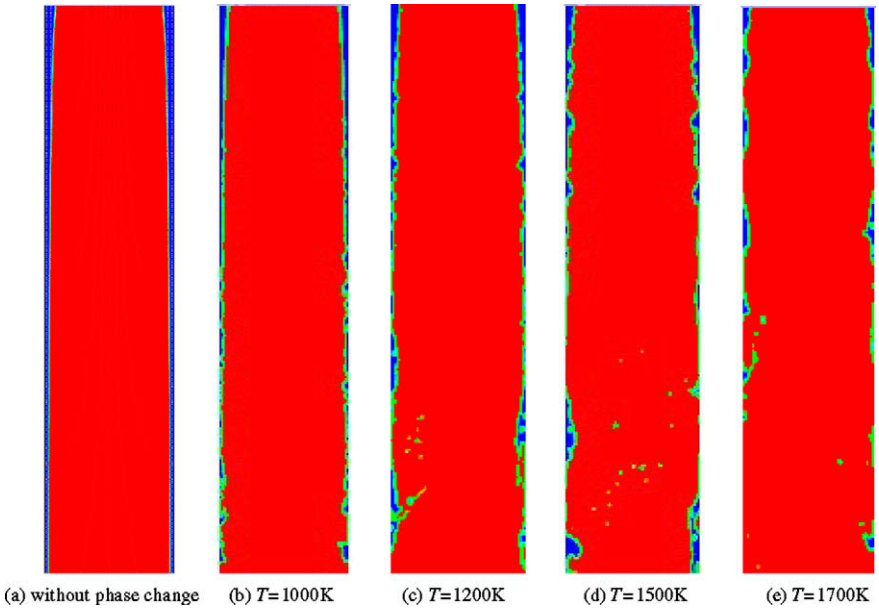

Fig. 3. Gas–liquid structure in the vertical pipe at various conditions.

the gas inlet temperature increases. For cases at $T = 1500$ K and $T = 1700$ K, the phenomenon of serious dry-out occurs with the wall exposed to the high-temperature syngas, which is tremendously detrimental to the gasification process. Simultaneously, the entrained droplets produced in the falling film disruption lead to the reduction of liquid flow rate along the wall, which instead accelerates the falling film rupture, as presented in Fig. 3(c–e).

3. Free surface flows in liquid–liquid systems

Free surface flows are types of fluid flows in which at least a portion of the surface bounding the domain of interest changes its shape as time elapses or a parameter is varied. Two common types of free surface flows are those involving liquid jets and drop formation. Such flows have been widely studied for more than a century due to their great importance in industrial processes, such as microencapsulation, inkjet printing, mixing and emulsion formation, fiber spinning and heat and mass transfer applications. Much of the earlier literature has been reviewed by Shi et al. (1994), Richards et al. (1993, 1994, 1995), and more recently by Milosevic and Longmire (2002), Doshi (2003) and Carsten et al. (2004). However, most of these studies were focused on the gas–liquid system. Due to the difference in physicochemical properties of the ambient fluid, such as dynamic viscosity, interfacial tension coefficient, weight, etc., there is quite a difference between drop formation in gas–liquid and liquid–liquid systems (Zhang and Basaran, 1995; Zhang and Stone, 1997; Zhang, 1999a; Doshi, 2003). Study of drop formation in liquid–liquid system is still largely lacking (Doshi, 2003). The main objective of this section is to develop a general understanding of two-liquid drop formation, using both numerical and experimental approaches.

3.1. Mathematical formulation

The classic VOF/CSF (Hirt and Nichols, 1981; Brackbill et al., 1992) transient model based on the Eulerian volume tracking approach is utilized uniformly for free interface tracking. For the jet flow under high Reynolds numbers, initial simulations revealed that the Reynolds averaging turbulence approach overly damped the fine scales of atomization, showing only the larger waves and surface fluctuations without eventual jet disruption (Peng et al., 2008). Instead, the VOF/CSF coupled with LES method was established for simulation of drop formation at high Reynolds numbers.

Governing equations of 2-D VOF-LES comprise the continuity and momentum equations and the volume fraction equation. In particular, the subgrid scale model proposed by Smagorinsky (1963) was applied to account for the large scale momentum flux caused by the action of the small or unresolved scales. The surface tension was dealt with the continuum surface force (CSF) model. Moreover, the piecewise linear interface calculation (PLIC) scheme (Youngs, 1982) was utilized for interpolation near the interface. The transient Navier–Strokes system was solved by using a finite-difference formulation on an Eulerian mesh.

3.2. Experimental approach

Experimental facility consisted essentially of a fine-capillary spray nozzle through which the liquid used to form drops was delivered at a constant volumetric flowrate by means of a booster bump. The inner diameter of the spray nozzle that was directed upwards, was 0.12 mm and the outer diameter was 0.3 mm. A steady, non-pulsating flow of the continuous phase was generated using a centrifugal pump, and finally entered a vertical transparent glass-pipe having a sufficiently large inner radius as compared with the nozzle radius so that the wall effects could be neglected (Zhang, 1999a,b). The continuum entered the pipe horizontally, about 300 mm below the spray nozzle tip in order to provide the steady laminar-flow of the external carrier fluid around the spay nozzle. The No. 25 transformer oil was selected as the carrier fluid. Usually, it appears transparent without any suspended matter, and has a viscosity and density of 0.179 kg $(\mathrm{m\,s})^{-1}$ and 895 kg m^{-3}, respectively. The interfacial tension coefficient between No. 25 oil and water was measured to be 0.062 N m^{-1} at room condition.

3.3. Results and discussion

Fig. 4 shows the bubbling regime of drop formation at low Reynolds number. In this regime, single drop forms, grows, and detaches from the nozzle at regular intervals. Drop formation is determined mainly by the balance mechanism of major forces:

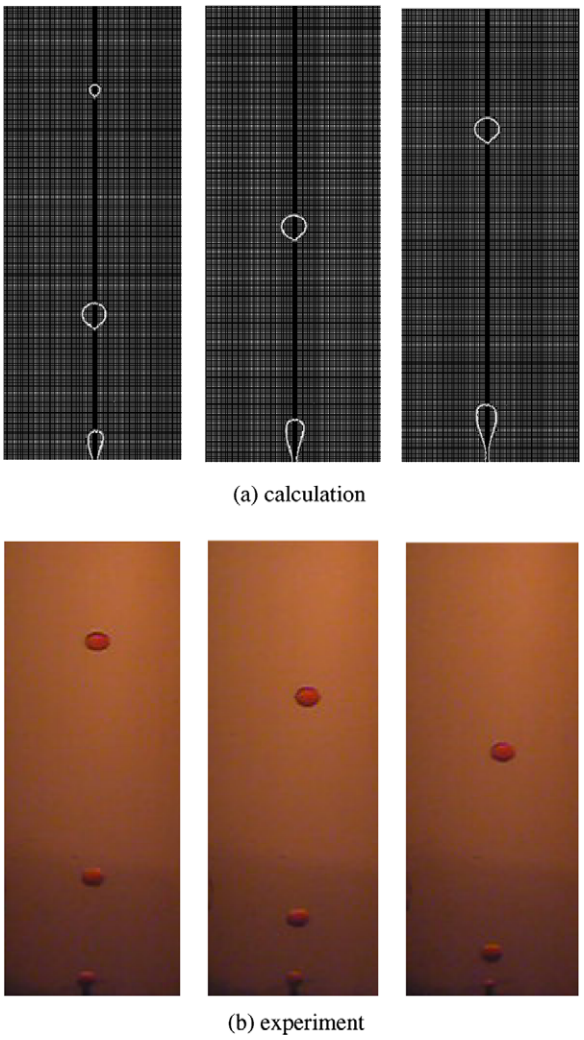

Fig. 4. Bubbling regime of drop formation when $v_{c,in} = 0.27$ m s^{-1} and $Re = 66$.

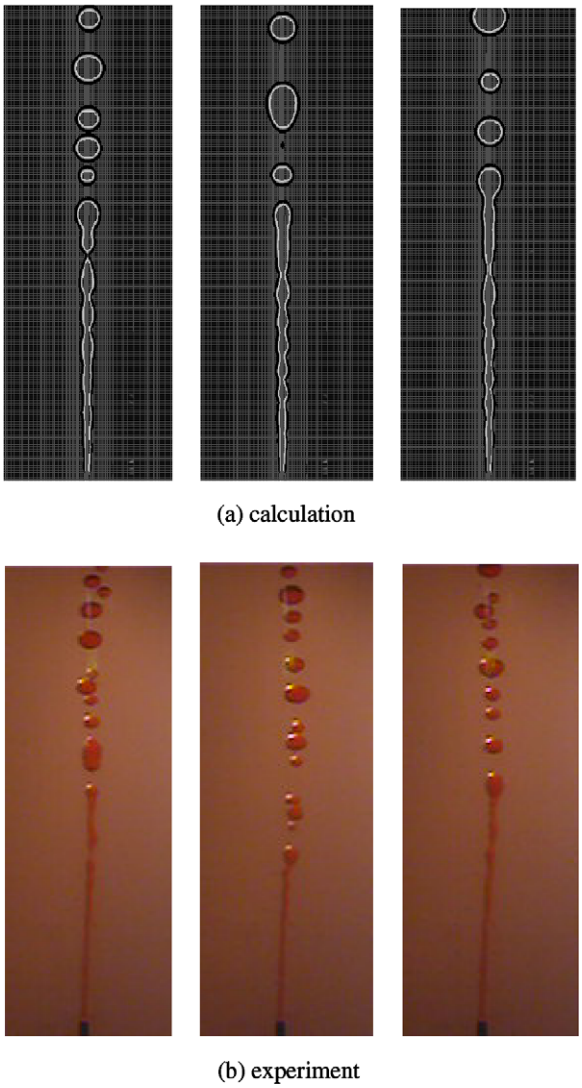

Fig. 5. Laminar jetting regime of drop formation at $v_{c,in} = 0.27$ m s^{-1}and $Re = 966$.

inertia, buoyancy, interfacial tension and viscosity (Scheele and Meister, 1968; Chen et al., 2001). This regime of drop formation was studied for the longest time, and currently, great progress has been made both theoretically and experimentally (Doshi, 2003). Fig. 4 shows the numerical results based on the laminar VOF/CSF model. Good agreement is achieved in comparison to the experimental results.

Fig. 5 illustrates the laminar jetting regime of drop formation. While the Reynolds number of the injection liquid exceeds a critical value, a jet streams from the nozzle, being laminar in flow. To a certain length, the jet breaks up into individual drop which flows upwards in line. Hereafter, the jet stability dynamics determine the mechanism and the size of the drops (Clift et al., 1978; Richards et al., 1994). For this regime, since the Reynolds number is relatively lower, the laminar VOF/CSF method neglecting the turbulence effects was still used. Good agreement was obtained between the predicted results and experimental observations. From Fig. 5, it can also be seen that the jet disrupts dynamically with length fluctuating with time in variable amplitudes. Similar results have been reported by Richards et al. (1994) and Carsten et al. (2004).

Fig. 6 shows the turbulent jetting regime of drop formation. In this regime, the jet becomes fully turbulent and eventually disrupts intensely into a large number of smaller drops. Both the modeling and the experiment illustrate the above phenomenon. In this case, the relative velocity between phases is so large that the shear stress plays a predominant role. Moreover, the radial and axial momentum in the jet is changed dramatically, which yields a sharp rise in the radial velocity (Liu and Reitz, 1993). Consequently, the jet disrupts intensely into a large number of smaller drops owing to the complicated factors mentioned above. As yet, there are very few publications focusing on this regime of drop formation in liquid–liquid systems. Discrepancies between the numerical and experimental results are primarily attributed to the 2-D model established, in which the eddy generation term is not comprised in the governing equations.

4. Mixing behavior of gas–liquid–solid three-phase flow

The system of gas–liquid–solid three-phase flow is commonly encountered in industrial fields. In the entrained-flow in Texaco gasifier stated in Section 2, coal–water–slurry or pulverized coal is gasified at high temperature and high pressure. Due to the subsequent severe heat and mass transfer with the falling film along the inside wall of the pipe, the syngas temperature declines steeply and the molten slag is solidified. In the cistern, heat is transferred severely again between phases. Finally, the scrubbed colder-syngas flows out of the cistern and the solidified slag subsides to the bottom.

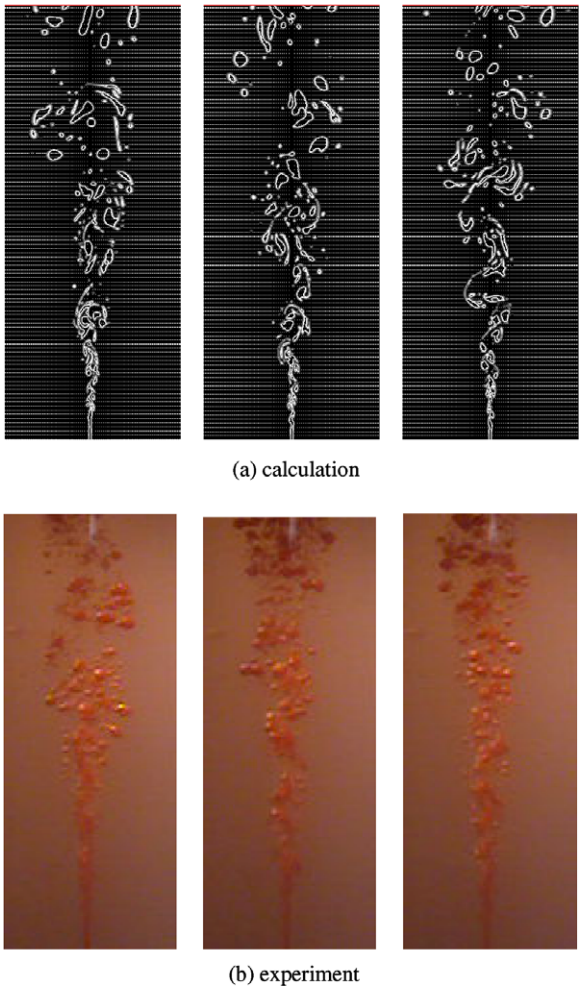

Fig. 6. Turbulent jetting regime of drop formation at $v_{c,in} = 0.27\ m\ s^{-1}$ and $Re = 4825$.

The scrubbing process is of great importance because the reactor performance determines the number and size of needed separation units before and after the reactor and, hence dictates the economics of the whole process. It is thus essential to quantify various measures of the scrubbing performance, such as complicated structure of the multiphase flow, particle concentration distribution, particle flow tendency, etc., as a function of the design and operating parameters.

4.1. Mathematical formulation

The CFD-VOF method coupled with discrete particle model (DPM), more advanced in comparison with that proposed by Li et al. (1999), was developed for simulation. The sampled particles were discretely treated in a Lagrangian manner and tracked throughout the domain, and the continuum was simulated by the classic Euler–Euler method, in specific the VOF model. The RNG κ–ε model was used to consider the turbulent quantities.

The motion of a particle in the liquid or gas phase was solved by Newton's second law of motion. As discussed in Wu et al. (2008), the spin-lift and Basset history forces were ignored. The modified Nanbu method (Tsuji et al., 1998; Zou et al., 2008) was improved to modify the collision probability, guaranteeing no more than one collision for each particle during a physical time step.

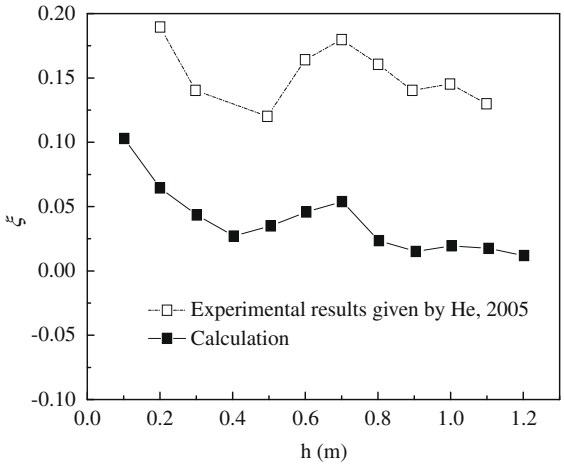

Fig. 7. Comparison of simulated and experimental results on mass-weighted ratio of the solid phase.

4.2. Results and discussion

Fig. 7 shows the numerical results of the mass-weighted ratio ξ of particles along the height of scrubbing–cooling chamber, compared with the experimental-data given by He (2005). Qualitatively, it can be seen that the numerical predictions agree well with the experimental results. However, there is a marked discrepancy in the observed results. Firstly, it can be attributed to the data acquisition approach in the experiments. In the work of He (2005), due to the limitation of measurement techniques the data obtained in experiments uniformly represents the mass-weighted ratio of particles in the liquid phase rather than in the gas–liquid mixture. Hence, the value is proportionally higher than that predicted by the numerical method. Secondly, the sampled particles were tracked and resolved in simulation to represent the solid phase flow (Tsuji et al., 1998; Zou et al., 2008). Due to the limitation of computational capabilities, the total number of particles involved in this simulation was fewer than in the actual experiments, and although the initial size distribution of the feeding particles was

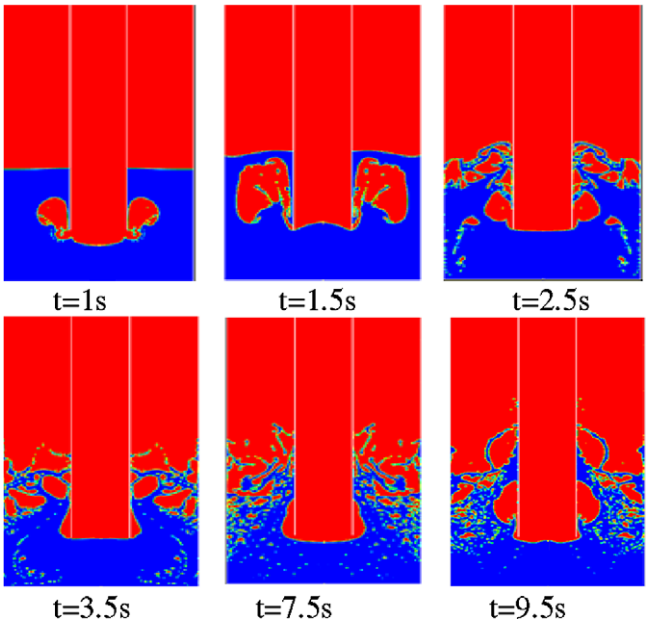

Fig. 8. Simulation results of gas–liquid two-phase flow field when $U_{sf} = 1.0\ m\ s^{-1}$.

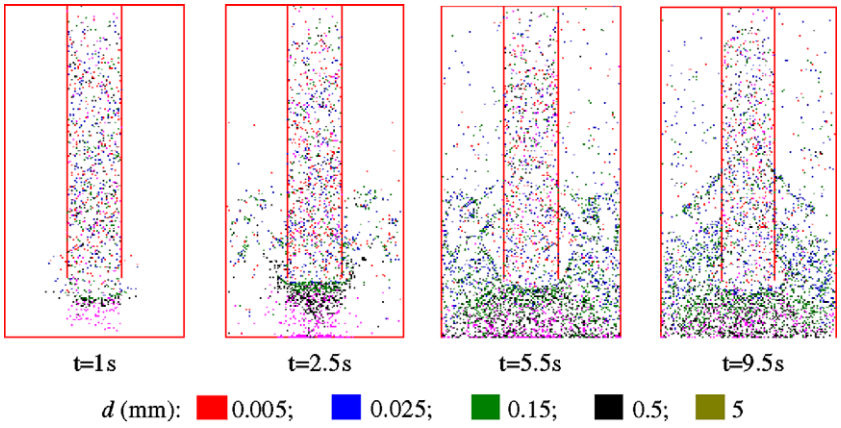

Fig. 9. Simulation results of spatial distribution of solid particles when U_{sf} = 1.0 m s^{-1}.

adjusted to be equivalent to that in experiments, inaccuracy could not be avoided.

Fig. 8 illustrates a time sequence of fluids flow in the cylindrical vessel after the syngas is injected into the cistern at a superficial velocity U_{sf} = 1.0 m s^{-1}. The red denotes the volume fraction distribution of the gas phase. It can be seen that the gas disrupts rapidly after entering the cistern, which was also reported by Liovic et al. (2002). The dispersed droplets are entrained by bubbles, splashing over the quiescent free surface. Coalescence and breakup of bubbles and droplets occur frequently below the surface due to the intense momentum exchange between phases. Moreover, no bubbles or droplets consistently move in single well-defined trajectories in the chamber, appearing fairly chaotic.

Fig. 9 shows the corresponding instantaneous spatial distribution of solid particles in different size in the chamber. Bigger particles are accumulated at the bottom, whereas small particles concentrate either around the outlet of the cooling tube or near the surface of the external liquid. Some of the fine particles escape from the cistern together with the dispersed bubbles and droplets.

5. Fluidization behavior of cylindrical particles in gas–solid flow

Nowadays, the fluidized straw combustion has been accepted as a promising technique due to its technical merits including high combustion efficiency, wide combustion adaptability, easy temperature control and low emission of pollutants (Cui and John, 2006). In the past two decades, the technology of fluidized straws direct combustion has developed rapidly. However, a comprehensive understanding of the mechanisms in the cylindrical-particle-laden two-phase flows is still lacking (Zak, 2001; Lin et al., 2003). In the few numerical studies, moreover, the solid-phase is generally treated simply as a spherical particle. Such a simplification can lead to large errors when predicting the cylindrical-particle motion. In this paper, a three-dimensional rigid dynamics model is developed to investigate the fluidization behavior of the cylindrical particles in gas–solid flow, including fluid dynamics, rigid dynamics and rigid collision dynamics.

5.1. Mathematical formulation

The kinetics of body is introduced for analyses. Fluid drag force acting on part i of a cylindrical particle is:

$$\boldsymbol{F}_{fi} = C_D A_c \rho_f |\boldsymbol{u}_f - \boldsymbol{u}_i|(\boldsymbol{u}_f - \boldsymbol{u}_i)/2 \tag{6}$$

where, C_D is the drag coefficient; A_c is the cross-section area of the part; ρ_f is the fluid density; $\boldsymbol{u}_f$ is the fluid velocity; $\boldsymbol{u}_i$ is the particle part velocity, $\boldsymbol{u}_i = \boldsymbol{u}_0 + (\boldsymbol{I}\cdot\omega)\times r_i$, $\boldsymbol{u}_0$ is the velocity on the centroid of the cylindrical particle.

The drag coefficient C_D in traditional calculations that was always used for spherical particles will result in large errors for simulation of the cylindrical particles motion. A new calculation model of C_D, based on the work of Hottovy and Sylvester (1979) and Tran-Cong et al. (2004) was introduced. In order to avoid the numerical singularity in kinetic calculation, the Euler parameters, λ_{0-3}, are introduced with the following relationship:

$$\lambda_0^2 + \lambda_1^2 + \lambda_2^2 + \lambda_3^2 = 1 \tag{7}$$

and can be calculated as:

$$\lambda_0 = \cos\left(\frac{\theta}{2}\right)\cos\left(\frac{\psi+\varphi}{2}\right),\quad \lambda_1 = \sin\left(\frac{\theta}{2}\right)\cos\left(\frac{\psi-\varphi}{2}\right)\quad \lambda_2 = \sin\left(\frac{\theta}{2}\right)\sin\left(\frac{\psi-\varphi}{2}\right),\quad \lambda_3 = \cos\left(\frac{\theta}{2}\right)\sin\left(\frac{\psi+\varphi}{2}\right) \tag{8}$$

where ψ, θ, φ are Euler angles, i.e., procession angle, nutation angle and rotation angle, respectively, which uniquely describe the polymorphism of the cylindrical particle in the bed.

The collision probability in the DSMC method given by Tsuji et al. (1998) was modified. The post-collision translational velocity and rotational velocity of the cylindrical particles were calculated based on the law of momentum conservation, details of which could be found in Cai et al. (2008).

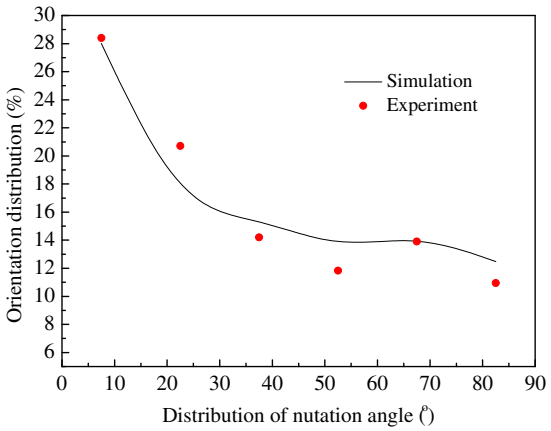

Fig. 10. Results of orientation distribution of cylindrical particles when gas superfacial velocity: U_{sf} = 4.5 m s^{-1}, particle slenderness: λ = 10, and solid flow rate: W = 0.27 kg s^{-1}.

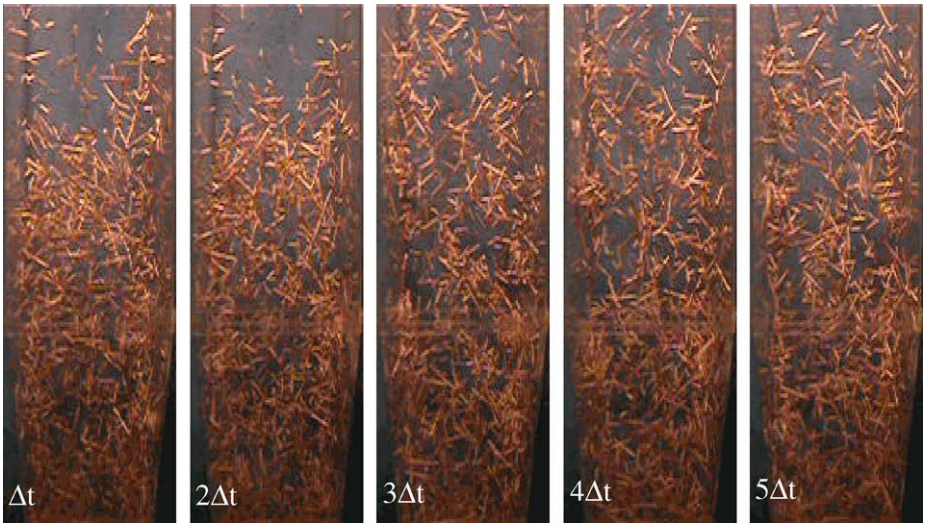

Fig. 11. Experiment snapshots of cylindrical particles fluidization with multi-slenderness: $\Delta t = 0.2$ s; $U_{sf} = 4.5$ m s^{-1}; $W = 0.27$ kg s^{-1}; $\lambda = 6, 8, 10$.

5.2. Experimental approach

The visual experimental system included fluidized bed, air providing source and high-speed digital photographing system. The fluidized bed was made of a glass pipe with square cross-section, and consisted of upside, middle part and nether part, totally 1.64 m in height. The cubic room for wind distribution was located just under the riser. The uniform size of the holes on the perforated plate was 1 mm in diameter and the overall porosity of the plate was 0.3. A filter was used to cover the grid plate to increase the bed resistance and distribute air evenly. The high-resolution digital camera (Nikon 5000, Japan) with ultra-high speed continuous shooting mode (100 frames per second) was employed to attain data.

5.3. Results and discussion

The orientation distribution of the cylindrical particles is defined as the number ratio of the particles whose attitude angles belong to a certain range to that flowing in the entire bed (Folgar and Tucker, 1984; Bernstein and Shapiro, 1994; Lin et al., 2006). Orientation distribution is one of the most important parameters that characterize the fluidization behaviors of cylindrical particles. In this paper, the nutation angle θ, which ranges from 0 to $\pi/2$, is divided into 6 parts evenly, and the two limits of $\theta = 0$ and $\theta = \pi/2$ correspond to the cases when the cylindrical particle is located vertically and horizontally in the bed, respectively. Fig. 10 shows the simulated results using the established model and the experimental results under the same conditions. As shown in Fig. 10, it can be found that the simulated results, in which most of the cylindrical particles move with small nutation angles in the riser, agree well with the experimental results.

Slenderness of the cylindrical particle refers to the ratio of particle length to particle diameter. Fig. 11 shows the experimental snapshots of flow patterns of the cylindrical particles with different slendernesses. It can be seen that the cylindrical particles with small-slenderness firstly reach the outlet of fluidized bed from the nearby regions of wall, where the particle concentration is accordingly higher than that in the radial centre region. Additionally, there is an evident phenomenon of particle floc during the fluidization.

Acknowledgments

This work was supported by the Major State Basic Research Development Program of China (2004CB217707) and Research Fund for the Doctoral Program of Higher Education of China (20060286034).

References

Bernstein, O., Shapiro, M., 1994. Direct determination of the orientation distribution function of cylindrical particles immersed in laminar and turbulent shear flows. J. Aerosol Sci. 25, 113–136.
Brackbill, J.U., Kothe, D.B., Zemach, C., 1992. A continuum method for modeling surface tension. J. Comput. Phys. 100, 335–354.
Brennen, C.E., 2005. Fundamentals of Multiphase Flow. Cambridge University Press.
Cai, J., Fan, F.X., Wu, X., Yuan, Z.L., 2008. Effects of inter-particle collisions on the orientation distribution of slender particles in gas–solid flows. Proc. Chin. Soc. Electr. Eng. 28, 66–69.
Carsten, C., Peter, F., Erich, J.W., 2004. Drop formation in a co-flowing ambient fluid. Chem. Eng. Sci. 59, 3045–3058.
Chen, C.T., Maa, J.R., Yang, Y.M., Chang, C.H., 2001. Drop formation from flat tip nozzles in liquid–liquid system. Int. Commun. Heat Mass Transfer 28, 681–692.
Clift, R., Grace, J.R., Weber, M.E., 1978. Bubbles, Drops, and Particles. Academic Press, New York.
Cui, H.P., John, R.G., 2006. Fluidization of biomass particles: a review of experimental multiphase flow aspects. Chem. Eng. Sci. 62, 45–55.
Dhanunjay, S.B., 2003. Simulation of granular and gas–solid flows using discrete element method. Ph.D. thesis, Carnegie Mellon University, Pittsburgh..
Doshi, P., 2003. Deformation and breakup of liquid–liquid threads, jets, and drops. Ph.D. Thesis, Purdue University, USA..
Folgar, F.P., Tucker, C.L., 1984. Orientation behavior of fibers in concentrated suspensions. J. Reinf. Plast. Comp. 3, 98–119.
He, B.Y., 2005. Study on multiphase flow characteristics of the new type of scrubbing–cooling chamber. Ph.D. thesis, East China University of Science & Technology, Shanghai..
Hiroki, Y., Fumio, K., Hideo, T., Akihiro, Y., Keiichi, O., Tadashi, M., 2008. Two-stage equilibrium model for a coal gasifier to predict the accurate carbon conversion in hydrogen production. Fuel 87, 2186–2193.
Hirt, C.W., Nichols, B.D., 1981. Volume of fluid (VOF) method for the dynamic of free boundaries. J. Comput. Phys. 39, 201–225.
Hottovy, J., Sylvester, D., 1979. Drag coefficients for irregularly shaped particles. Ind. Eng. Chem. Process Design Dev. 18, 433–436.
Hughes, D.T., Bott, T.R., 1998. Minimum thickness of a liquid film flowing down a vertical tube. Int. J. Heat Mass Transfer 41, 253–260.
Le, M., Hassan, I., 2007. DSMC simulation of gas mixing in T-shape micro-mixer. Appl. Therm. Eng. 27, 2370–2377.
Li, Y., Zhang, J.P., Fan, L.S., 1999. Numerical simulation of gas–liquid–solid fluidization systems using a combined CFD–VOF–DPM method: bubble wake behavior. Chem. Eng. Sci. 54, 5101–5107.
Lin, J.Z., Shi, X., Yu, Z.S., 2003. The motion of fibers in an evolving mixing layer. Int. J. Multiphase Flow 29, 1355–1372.
Lin, J.Z., Zhang, L.X., Zhang, W.F., 2006. Rheological behaviors of fiber suspensions in a turbulent channel flow. J. Colloid Interface Sci. 296, 721–728.
Liovic, P., Rudman, M., Liow, J.L., 2002. Numerical modeling of free surface flows in metallurgical vessels. Appl. Math. Model. 26, 113–140.
Liu, A.B., Reitz, R.D., 1993. Mechanism of air assisted liquid atomization. Atomization Sprays 3, 55–75.
Marco, F., 1995. A simple model to evaluate direct contact heat transfer and flow characteristics in annular two-phase flow. Int. J. Heat Fluid Flow 16, 272–279.

Milosevic, I.N., Longmire, E.K., 2002. Pinch-off modes and satellite formation in liquid–liquid jet systems. Int. J. Multiphase Flow 28, 1853–1869.
Peng, Z.B., Yuan, Z.L., Chen, P., He, Z.C., 2008. Three-dimensional simulation of liquid–liquid drop formation after jetting at low Reynolds numbers. International Pre-Olympic Workshop on Modelling and Simulation, Nanjing, 2008, vol. V, pp. 396–405..
Richards, J.R., Beris, A.N., Lenhoff, A.M., 1993. Steady laminar flow of liquid–liquid jets at high Reynolds numbers. Phys. Fluids A5, 1703–1717.
Richards, J.R., Lenhoff, A.M., Beris, A.N., 1994. Dynamic breakup of liquid–liquid jets. Phys. Fluids 6, 2640–2655.
Richards, J.R., Beris, A.N., Lenhoff, A.M., 1995. Drop formation in liquid–liquid systems before and after jetting. Phys. Fluids 11, 2617–2630.
Scheele, G., Meister, B., 1968. Drop formation at low velocities in liquid–liquid systems. AIChE J. 14, 9–15.
Shi, X.D., Brenner, M.P., Nagel, S.R., 1994. A cascade of structure in a drop falling from a faucet. Science 265, 219–222.
Siegel, R., Howell, J.R., 1992. Thermal Radiation Heat Transfer. Hemisphere Publishing Corporation, Washington, DC.
Smagorinsky, J., 1963. General circulation experiments with the primitive equations. I. The basic experiment. Mon. Weather Rev. 91, 99–164.
Tran-Cong, S., Gay, M.G., Michaelides, E.E., 2004. Drag coefficients of irregularly shaped particles. Powder Technol. 139, 21–32.
Tryggvason, G., Esmaeeli, A., Al-Rawahi, N., 2005. Direct numerical simulations of flows with phase change. Comput. Struct. 83, 445–453.
Tsuji, Y., Kawaguchi, T., Tanaka, T., 1993. Discrete particle simulation of two-dimensional fluidized bed. Powder Technol. 77, 79–87.
Tsuji, Y., Tanaka, T., Yonemura, S., 1998. Cluster patterns in circulating fluidized beds predicted by numerical simulation (discrete particle model versus two-fluid model). Powder Technol. 95, 254–264.
Wu, X., Li, T., Cai, J., Yuan, Z.L., 2008. Numerical simulation of particles distribution in process of gas crossing cistern in scrubbing chamber. Proc. Chin. Soc. Electr. Eng. 28, 16–19.
Youngs, D.L., 1982. Time-Dependent Multi-Material Flow with Large Fluid Distortion. Academic, New York.
Yuan, Z.L., 2000. Direct numerical simulation of dense gas–solid two-phase flows. Dev. Chem. Eng. Miner. Precess. 8, 207–217.
Zak, G., 2001. Estimation of three-dimensional fiber-orientation distribution in short-fiber composites by a two-section method. J. Compos. Mater. 35, 316–330.
Zhang, X., 1999a. Dynamics of drop formation in viscous flows. Chem. Eng. Sci. 54, 1759–1774.
Zhang, X., 1999b. Dynamics of growth and breakup of viscous pendant drops into air. J. Colloid Interface Sci. 212, 107–122.
Zhang, X.G., Basaran, O.A., 1995. An experimental-study of dynamics of drop formation. Phys. Fluids 7, 1184–1203.
Zhang, D.F., Stone, H.A., 1997. Drop formation in viscous flows at a vertical capillary tube. Phys. Fluids 9, 2234–2242.
Zou, L.M., Guo, Y.C., Chan, C.K., 2008. Cluster-based drag coefficient model for simulating gas–solid flow in a fast-fluidized bed. Chem. Eng. Sci. 63, 1052–1061.